www.sciencemag.org/content/363/6431/eaav7932/suppl/DC1

Supplementary Materials for

Exotic states in a simple network of nanoelectromechanical oscillators

Matthew H. Matheny, Jeffrey Emenheiser, Warren Fon, Airlie Chapman, Anastasiya Salova, Martin Rohden, Jarvis Li, Mathias Hudoba de Badyn, Márton Pósfai, Leonardo Duenas-Osorio, Mehran Mesbahi, James P. Crutchfield, M. C. Cross, Raissa M. D'Souza, Michael L. Roukes*

*Corresponding author. Email: roukes@caltech.edu

Published 8 March 2019, *Science* **363**, eaav7932 (2019)
DOI: 10.1126/science.aav7932

This PDF file includes:

Other supplementary material for this manuscript includes:

Movies S1 to S32 (as identified in Tables S1 to S3)

Materials and Methods

NEMS resonator and oscillator

A ring network of 8 nanomechanical oscillators was constructed. In each oscillator, a nanoelectromechanical resonator was bonded onto a printed circuit board hosting the control and feedback electronics. A scanning electron micrograph of the resonator (with false color added for clarification of the device structures) is shown in Fig. S1A, top. It is an ultrathin fully clamped plate with an embedded aluminum nitride piezoelectric film (30,61). Each plate had a resonant frequency set to $f_m = 2.21000 \pm .00002$ MHz with a quality factor $Q_m = 3950 \pm 550$. The resonator clamping gave a geometric Duffing-type nonlinearity (37) and the capability of linear voltage-frequency tuning (62). The resonators were mounted inside a vacuum chamber and wirebonded onto a printed circuit board (PCB) (Fig. S1B) to form the self-sustained oscillator. Fon, et al. (30) gives the details for the oscillator circuit. Tuning of resonator frequency (and therefore natural oscillator frequency ω_j) and nonlinearity α were done with an on-board 16-bit ultrastable Digital-to-Analog-Converter (DAC) (white box in Fig S1B) and a 7-bit variable attenuator (blue box in Fig. S1B), respectively.

Network construction

The oscillator PCB was connected through an edge connector to the network (purple box in Fig. S1B). The network PCB connected the 8 oscillators into a ring topology so that each oscillator was coupled to their two nearest neighbors (Fig. S1C). The network PCB had variable attenuators controlling the strength (and to ensure the proper phase shift through the oscillator loop) of coupling β along the edges (yellow box in Fig. S1D). Power and digital control signals were directly provided to the network PCB and routed to the oscillator boards. Even though our controls were adjusted via digital commands, signals passing between the nodes and edges were analog signals and never digitized, and our network evolves according to a continuous time dynamic.

Data acquisition, control, and calibration

Python scripts were used for taking and analyzing data. Python libraries were also used for numerical simulations.

A personal computer (PC) was connected to a digital controller (Raspberry Pi) (dark blue box in Fig. S1D) via Ethernet. Python scripts used C libraries within the controller which switched settings within digital potentiometers, variable attenuators, and DACs within our network. The electronic components (DACs and attenuators) controlled the natural frequencies ω_j, nonlinearities α, and couplings strengths β of the nodes and edges. Every node and edge were comprised of their own components which could be individually addressed by the controller. In addition, each node was readout in an individual channel of a simultaneous-sampling 8-channel oscilloscope.

In Eq. 2b (main text), when the j^{th} oscillator was isolated such that $a_{j+1}, a_{j-1} = 0$, we see that changes in α, β, and ω_j are associated with changes in its frequency. Each node's

parameters were individually calibrated with measurement of the isolated oscillator frequency for a given choice of parameters. The scaling of these parameters was either linear or quadratic in PCB signals. Quadratic and linear fits yielded a simple calibration for the parameters; these fits eliminated the need for lookup tables. We refer the reader to Matheny, et al. (14) for more details on the calibration.

In order to maintain throughput in data acquisition and storage, the 'fast' oscillator signals (at ~2 MHz) were captured with full fidelity in the system calibration but subsequently undersampled at 200 kHz. Note that since the slow time scale was $\tau_{slow} \approx \frac{Q_m}{f_m} \approx 2$ ms in our experiment, our sampling frequency was $\sim 1000\times$ that of the Nyquist limit relative to the evolution of the slow time complex amplitude in Eq. 1, main text. We perform the Hilbert transform on the raw time-domain signal, $H[V_j(t)]$, and extract the angle to acquire the phase (63). The magnitudes a_j are the magnitudes of the transformed signals, normalized by the magnitudes when oscillators are isolated, $\left|H\left[V_j(t)\right]\right|/\left|H[V_j(t=0)]\right|$ (with the system uncoupled at $t = 0$) . The phases are further binned and averaged by a factor of 40 to smooth the time domain data.

Supplementary Text

Additional exotic states

When $\beta < 1$ and $\alpha > 0.06$ the experimental system exhibits additional states of interest – several kinds of traveling waves and a noise-driven chimera. The following sections describe these briefly.

The system exhibited additional traveling wave states other than those outlined in the main text. Figure S2A displays a traveling wave state centered around the k = 2,6 fixed points. It consists of a smooth, sinusoidal variation in the phase difference, much like the main text's 2-TW-I state. In contrast to the 2-TW-I state, we observed a spatial wavevector of $\pi/4$. This state was found to be stable in the simulation when the parametric interactions (described later in the supplementary text) were added.

Figure S1B shows a pulse in the phase difference which propagated around the ring. We found a similar state to occur in the main text's 2nd order phase model. In Fig. S2C, we plot a complex traveling wave state. This state did not appear in the 2nd order phase model, and was only stable at large coupling and low nonlinearity, $\beta > 0.7, \alpha < 0.1$.

We also found a chimera-like state. Various definitions of "chimera" on a finite network have been proposed (45,46). Here we show a state that has two types of clusters: one type that was coherent and stable in time and another that was sensitive to noise and appears to drift. It differs from the "weak chimeras" mentioned in the main text.

The state's experimental data appears in Fig. S3. Figure S3A shows that the state consists of two locked pairs of phase difference: two at high frequency and two at low frequency. These pairs were in an antiphase configuration (see Movie S15 in the Supplementary Material). Between these pairs were noisy oscillators, which regularly jump by odd

multiples of π, as shown in Fig. S3 B and D. These jumps occurred when the neighboring phases were antiparallel. Oscillators across the ring were usually π out of phase at most times, with occasional 2π slips between noisy pairs.

This state has at least three frequencies (and hence the invariant subspace must be greater than 2 dimensional) and antiphase correlations between the stable oscillators. It shows a pattern {a,b,c,d,-a,-b,-c,-d} and has the symmetry of the isotropy subgroup $Z_2(p = 1)$. This state was only stable at higher values of coupling $\beta > 0.7$. In this state, a small amount of noise shifts the absolute phase of the noisy oscillators. The noisy oscillators synchronized for short periods of time, between periodic slips at random distance (Fig. S3D).

Figure S3E shows the long-term deviation of three oscillators, $\delta\phi_j = \phi_j - \Omega_j t$. We saw that there was no long-term drift of phase for oscillator 3, but oscillators 2 and 4 performed random walks. The walks were seemingly driven by noise, since they did not appear in deterministic simulations (not shown). There, the `noisy' oscillators slipped regularly in the sequence $\{\pi, -\pi, \pi, -\pi, ...\}$. Despite the presence of noise, we call this state a chimera since there was a coherent set of oscillators and an incoherent set.

Stability of splay states and pattern formation within inhomogeneous synchronized states

Next, we examine the stability of the splay states. While done in Emenheiser, et al. (32), here we derive the result differently to elucidate the formation of the patterns in the main text's discussion of inhomogeneous synchronization.

Absent frequency disorder, starting from the equations for the magnitudes and phase differences (see the main text for the starting complex amplitude equation),

$$\begin{aligned}\frac{da_j}{dT} = \dot{a}_j &= \frac{1-a_j}{2} - \frac{\beta}{2}\left[a_{j+1}\sin\Delta_j - a_{j-1}\sin\Delta_{j-1}\right] \\ \frac{d\Delta_j}{dT} = \dot{\Delta}_j &= \alpha\left(a_{j+1}^2 - a_j^2\right) \\ &\quad + \frac{\beta}{2}\left[\left(\frac{a_j}{a_{j+1}} - \frac{a_{j+1}}{a_j}\right)\cos\Delta_j + \frac{a_{j+2}}{a_{j+1}}\cos\Delta_{j+1} - \frac{a_{j-1}}{a_j}\cos\Delta_{j-1}\right]\end{aligned} \tag{S1}$$

with $\Delta_j = \phi_{j+1} - \phi_j$ as in the main text.

Each splay state has a fixed phase difference $\Delta_j = \Delta = \frac{2\pi k}{N}$ (with k={0,1,...,N-1} for N oscillators) and a magnitude $a_j = 1$. Thus, the stability of each state is given by,

$$\delta\dot{a}_j = -\frac{a_j}{2} - \frac{\beta}{2}\sin\Delta\left(\delta a_{j+1} - \delta a_{j-1}\right) - \frac{\beta}{2}\cos\Delta\left(\delta\Delta_j - \delta\Delta_{j-1}\right) \tag{S2}$$

$$\begin{aligned}\delta\dot{\Delta}_j = 2\alpha\big(\delta a_{j+1} - \delta a_j\big) \\ + \frac{\beta}{2}\big[\big(3\delta a_j - 3\delta a_{j+1} + \delta a_{j+2} - \delta a_{j-1}\big)\cos\Delta \\ - \big(\delta\Delta_{j+1} - \delta\Delta_{j-1}\big)\sin\Delta\big]\end{aligned}$$

Assuming variations in the state take the form of plane waves $\delta a_j = \delta a\, e^{iQj} e^{\sigma t}$, $\delta\Delta_j = \delta\Delta\, e^{iQ(j+1)} e^{\sigma t}$ with spatial wavevector Q and inserting into Eq. S2, we get,

$$\begin{aligned}\sigma\delta a &= \frac{\delta a}{2}\big[-1 - \beta\sin\Delta\big(e^{iQ} - e^{-iQ}\big)\big] - \frac{\beta}{2}\cos\Delta\,\delta\Delta\left(e^{\frac{iQ}{2}} - e^{-\frac{iQ}{2}}\right) \\ \sigma\delta\Delta &= 2\alpha\delta a\left(e^{\frac{iQ}{2}} - e^{-\frac{iQ}{2}}\right) \\ &\quad + \frac{\beta}{2}\left[\cos\Delta\,\delta a\left(3e^{-\frac{iQ}{2}} - 3e^{\frac{iQ}{2}} + e^{\frac{3iQ}{2}} - e^{-\frac{3iQ}{2}}\right)\right. \\ &\quad \left. - \sin\Delta\delta\Delta\left(e^{iQ} - e^{-iQ}\right)\right]\end{aligned} \tag{S3}$$

This gives a stability matrix of the form,

$$\begin{bmatrix} \sigma + \frac{1}{2} + i\beta\sin\Delta\sin Q & i\beta\cos\Delta\sin\frac{Q}{2} \\ -4i\alpha\sin\frac{Q}{2} - i\beta\cos\Delta\left(\sin\frac{3Q}{2} - 3\sin\frac{Q}{2}\right) & \sigma + i\beta\sin\Delta\sin Q \end{bmatrix} \tag{S4}$$

whose determinant yields solutions of the form,

$$\sigma = -i\beta\sin\Delta\sin Q + \frac{1}{4}\left[1 \pm \sqrt{1 + 64\beta\cos\Delta\sin^2\frac{Q}{2}\left(\alpha - \beta\cos\Delta\sin^2\frac{Q}{2}\right)}\right] \tag{S5}$$

For the pattern forming states (such as the inhomogeneous states from the main text), from a quench we expect the mode which was established to be the one with the maximum growth rate Γ from the real part of Eq. S5. Maximizing with respect to the wavevector yields $Q = 2\sin^{-1}\sqrt{\alpha/2\beta}$. For a single period (wavevector $Q = \frac{\pi}{4}$), the instability occurs when $\alpha = \beta\cos\Delta\sin^2\pi/8$. The same result was found in Emenheiser, et al. (32).

A two-period mode with a wavelength of 4 oscillators ($Q = \pi/2$) becomes unstable for $\alpha > \beta/2$. However, the inhomogeneous states were not found to be stable in the simulations for such parameter values (see Fig. 3C, main text). Thus, for the inhomogeneous states (developing from the uniform in-phase state) on the 8-ring we expect (and we found) that all the patterns have a single period. Thus, the only inhomogeneous state we found arising from the in-phase state was the pattern with a wavelength of 8 oscillators, corresponding to the first Fourier mode.

Origin of the decoupled traveling wave states

We establish the connection between a nonlinear coupling term and the decoupled traveling waves in this section.

Nonlinear coupling between the NEMS can be established via parametric terms driving neighboring oscillators. In Villanueva, et al. (15), it was shown that piezoelectric NEMS parametrically respond to harmonics of the feedback: feedback which tunes the frequency of the NEMS at twice the resonant frequency excites mechanical motion. Harmonics of the feedback can appear due to compression in the electronic circuits used for amplification of the small NEMS signal. We found that a second harmonic at the 5% level (compared to the first harmonic) generated the decoupled traveling wave states (2-TW-I) observed in the experimental oscillator ring.

Suppose that a term appears in the equation of motion for the displacement x_j of oscillator j,

$$\ddot{x}_j = \cdots + \zeta x_{j+1}^2 x_j \tag{S6}$$

where we have ignored the contribution from the $j-1$ oscillator (whose contribution can be added in a similar fashion at the end of the derivation). We are interested in the dynamics of Eq. S6 at the slow time scale (64,15,16,17). Assuming the displacement can be written as a slowly varying complex envelope on top of a fast waveform $x_j = A_j e^{i\omega t} + \bar{A}_j e^{-i\omega t}$,

$$\begin{aligned} 2i\omega\left(\dot{A}_j e^{i\omega t} - \dot{\bar{A}}_j e^{-i\omega t}\right) \\ = \cdots \\ + \zeta\left[\left|A_{j+1}^2\right| + A_{j+1}^2\, e^{2i\omega t} + \bar{A}_{j+1}^2\, e^{-2i\omega t}\right] \times \left[A_j e^{i\omega t} + \bar{A}_j e^{-i\omega t}\right] \end{aligned} \tag{S7}$$

where $\overline{A}_j$ is the conjugate of the complex amplitude A_j, and ω is the frequency of oscillation.

Gathering the secular terms at $e^{i\omega t}$, writing out $A_j = a_j e^{i\phi_j}$, and dividing through by $e^{i\phi_j}$ gives,

$$\begin{aligned} 2\omega\left(\dot{a}_j + i a_j \dot{\phi}_j\right) \\ = \cdots \\ - \zeta a_{j+1}^2 a_j\left[i\left(1 - \cos\left(2\left[\phi_{j+1} - \phi_j\right]\right)\right) + \sin\left(2\left[\phi_{j+1} - \phi_j\right]\right)\right] \end{aligned} \tag{S8}$$

which when inserted in the full magnitude-phase equation, normalizing the time by ω and putting in the $j-1$ terms,

$$\frac{da_j}{dT} = \frac{1-a_j}{2} - \frac{\beta}{2}\left[a_{j+1}\sin\left(\phi_{j+1}-\phi_j\right) + a_{j-1}\sin\left(\phi_{j-1}-\phi_j\right)\right] - \frac{\zeta a_j}{2}\left[a_{j+1}^2\sin\left(2\left[\phi_{j+1}-\phi_j\right]\right) + a_{j-1}^2\sin\left(2\left[\phi_{j-1}-\phi_j\right]\right)\right]$$

$$\frac{d\phi_j}{dT} = \alpha a_j^2 - \beta\left(1+\frac{\zeta}{2}\left[a_{j+1}^2+a_{j-1}^2\right]\right) + \frac{\beta}{2a_j}\left[a_{j+1}\cos\left(\phi_{j+1}-\phi_j\right) + a_{j-1}\cos\left(\phi_{j-1}-\phi_j\right)\right] - \frac{\zeta}{2}\left[a_{j+1}^2\cos\left(2\left[\phi_{j+1}-\phi_j\right]\right) + a_{j-1}^2\cos\left(2\left[\phi_{j-1}-\phi_j\right]\right)\right] \quad \text{(S9)}$$

Note that we have generated explicit higher harmonic phase coupling through these additional parametric coupling terms in the original equation of motion for the oscillators. For the appropriate choice of the sign of ζ, we found that these higher order couplings drove the trajectories away from the fixed points associated with $\Delta = \pi/2, 3\pi/2$. This created an instability since the trajectories would decay into these fixed points in the absence of this additional nonlinear parametric coupling.

We performed a numerical simulation of Eq. S9 with $\zeta = 0.05\beta$, and obtained behavior similar to that demonstrated by the experimental 2-TW-I state in the main text. The results are plotted in Fig. S4. These two plots can be qualitatively compared to the experimental data from Fig. 4B in the main text. Comparing the results quantitatively, the frequency of the oscillation in the phase differences found in simulation was within 5% of the experiment.

Simulations of the extended phase model

Here we show that the states found in experiment (except for the decoupled traveling wave and 0-TW-I states) were also found in simulations of the extended phase model. We have already shown a simulation of the WC-II state in the main text, so will not reproduce it here. Also, the splay states associated with $k = \{3,4,5\}$ are stable within the Kuramoto model, so we do not show these states either. All the plots in this section were composed with numerical data from simulations of Eq. (3) in the main text.

We start with the $k = \{0,1\}$ splay states (the $k = 7$ state has the same stability as the $k = 1$ state) and the inhomogeneous synchronized state. These are shown as phase difference plots in Fig. S5A-C. Incidentally, the only coupling beyond the Kuramoto-Sakaguchi terms in the phase model (with repulsive coupling) required for stabilizing the $k = 1$ were the triadic interactions. Likewise, only the biharmonic interactions were required for the in-phase state. In Fig. S5D, we show the pattern of phase differences for the data from C.

Next, we show simulations of the decoupled precessing state (2-precess) and the first weak chimera (WC-I). We only show the frequency space-time plots in Fig. S6, since the clustering can be immediately compared to the experimental data in the main text. We do not present the scale of the frequencies in the plots; these frequencies are determined by

the system's disorder (as in the 2-precess state) or were quantitatively incorrect (as in the WC-I state).

Simulations of the extended phase model

The supplementary movies show experimental data for states mentioned within the text and supplementary information. There are two representations in video form: "spin type" and "firefly type". In the spin type movies, oscillations are represented by arrows with angle corresponding to phase, and length corresponding to magnitude. In the firefly type, the phase of the oscillation is represented by a color on a cyclic color scale, with no representation of magnitude.

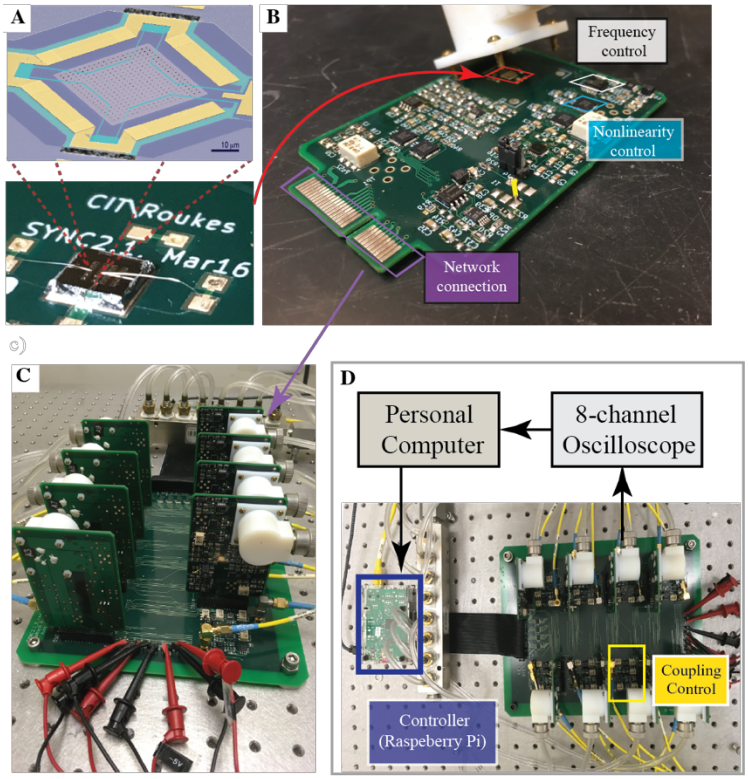

Fig. S1: Experimental setup. A) The ring network is constructed from eight individual piezoelectric plate resonators (SEM micrograph, top, with false color to contrast functional layers) with dimensions $area \times thickness = 1600\mu m^2 \times .145\mu m$. Each resonator is bonded (bottom) and housed in the white vacuum chamber on the oscillator printed circuit board (PCB). **B**) On the 'oscillator' board, the feedback to generate self-oscillation is applied. Controls for natural frequency and nonlinearity are shown by blue and white boxes. **C**) Eight oscillator boards are installed on the network board to form the ring network. **D**) Full diagram of the system. The PC sends digital commands to the controller over ethernet (dark blue box) who translates those commands to the digital bus (black cable) which connects to the network board. The data is read out via the yellow SMA cables and sent to an 8-channel oscilloscope. The controls for one edge are shown by the yellow box.

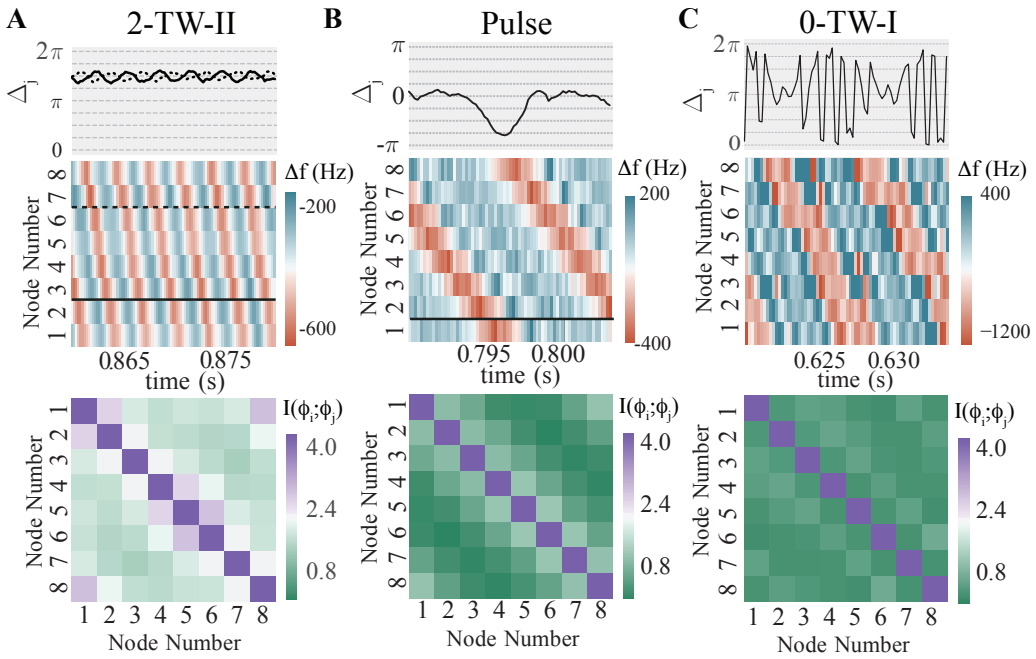

Fig. S2: Other traveling wave states. A) 2-TW-II. Additional traveling wave state around the $k = 2{,}6$ fixed points. It has a spatial wavevector of $\pi/4$. **B)** Phase pulse. **C)** Complex traveling wave state 0-TW-I.

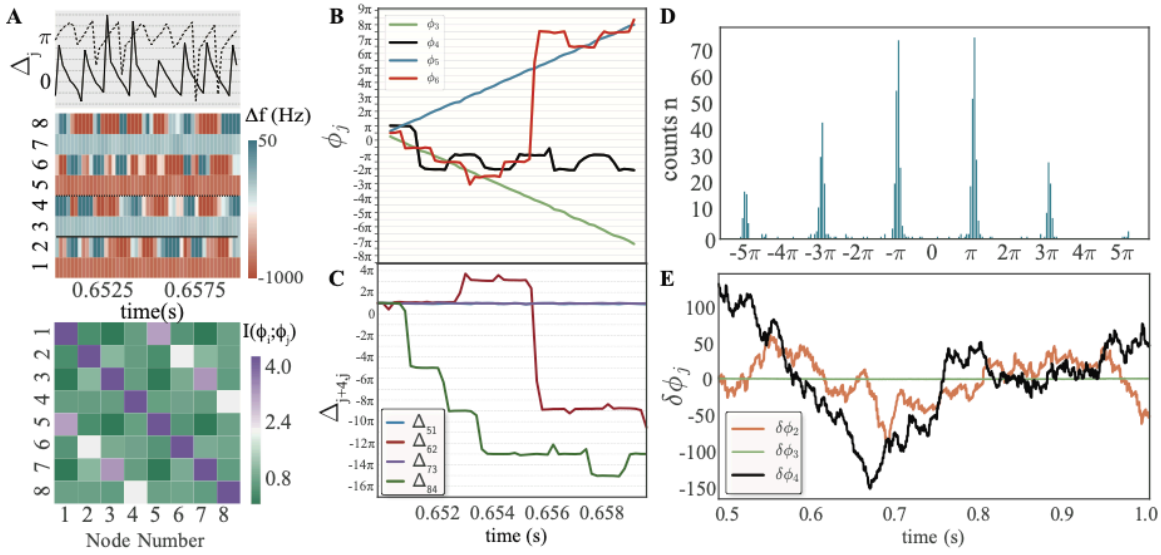

Fig. S3: Noise driven chimera. A) Phase differences, frequencies, and pairwise mutual information of the noisy chimera state. Note that the frequencies of 4 of the oscillators display aperiodic jumps in frequency. The mutual information shows a partial $\boldsymbol{Z_2}$ symmetry. **B**) We plot the phases of three of the oscillators in the rotating frame where the phase of oscillator 4 does not precess between slips. This shows that without slips, the oscillator is at the mean frequency of its neighbors. **C**) Phase differences across the ring show slips across the ring occur in steps of 2π. **D**) The histogram of oscillator events shows that all the phase slips are odd multiples of $\boldsymbol{\pi}$. The nonzero mean of the histogram shows that additional phase precession occurred due to these odd-π slips. **E**) The deviation of the phases from their mean precession ($\delta\phi_j = \phi_j - \Omega_j t$) shows that the noisy oscillators were highly unstable compared the locked oscillators and appear driven by noise

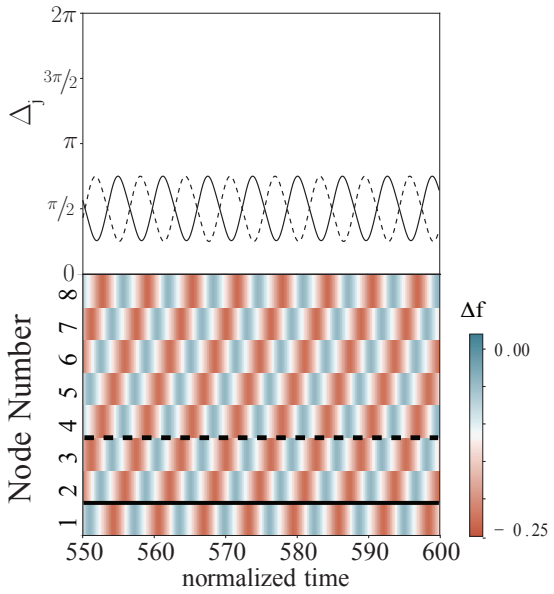

Fig. S4: Simulation of parametrically coupled ring. The simulation shows that two of the nearest neighbor phase differences (j=2 and j=4) have opposite phase and oscillate around $\frac{3\pi}{2}$ (top) and the space-time plot of frequencies shows the exact same wavevector as the experimental data (bot).

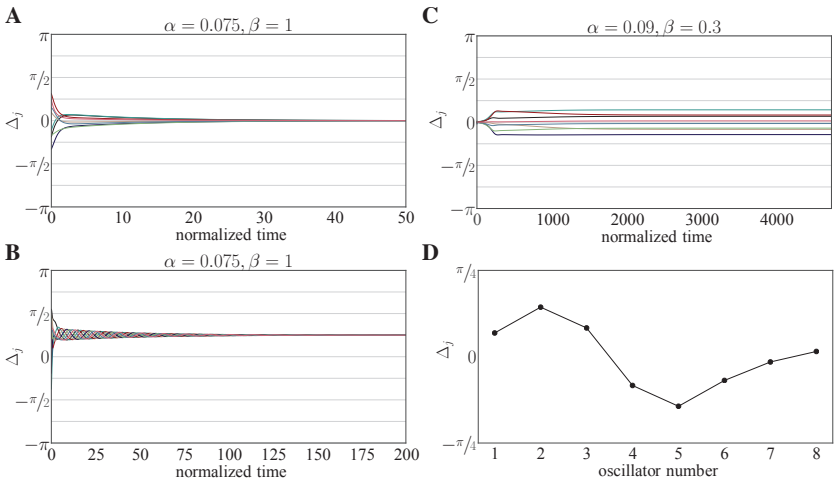

Fig. S5. Simulation of static states using the extended phase model. Phase differences from simulated data show stable in-phase states (**A**), or a stable k = 1 splay state (**B**). In (**C**) we see the phase differences relax to an inhomogeneous synchronized state. A pattern developed over a long period of time in the form shown in (**D**).

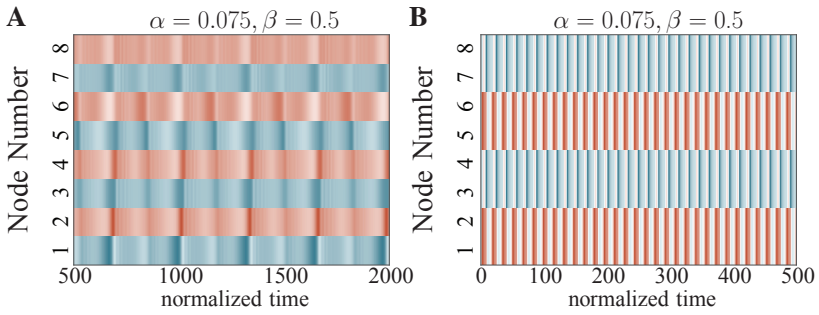

Fig. S6: Simulation of clustered states using the extended phase model. Frequency space-time plots of the 2-precess state (**A**), and the WC-I state (**B**) at $\alpha = 0.075, \beta = 0.5$.

Table S1.

Movies of the splay states from the main text.

State name	In-phase (k=0)	k=1	k=3	Antiphase (k=4)	k=5	k=7
Spin type	S1	S2	S3	S4	S5	S6
Firefly type	S17	S18	S19	S20	S21	S22

Table S2.

Movies of the exotic states from the main text.

State name	Inhomogeneous Synchronized	2-precess	2-TW-I	WC-I	WC-II
Spin type	S7	S8	S9	S10	S11
Firefly type	S23	S24	S25	S26	S27

Table S3.

Movies of the exotic states from the supplementary text.

State name	2-TW-II	Soliton	0-TW-I	Noise Driven Chimera	WC-II (in-phase type)
Spin type	S12	S13	S14	S15	S16
Firefly type	S28	S29	S30	S31	S32

References

1. C. Chen, S. Liu, X. Q. Shi, H. Chaté, Y. Wu, Weak synchronization and large-scale collective oscillation in dense bacterial suspensions. *Nature* **542**, 210–214 (2017). doi:10.1038/nature20817 Medline

2. I. Dinstein, K. Pierce, L. Eyler, S. Solso, R. Malach, M. Behrmann, E. Courchesne, Disrupted neural synchronization in toddlers with autism. *Neuron* **70**, 1218–1225 (2011). doi:10.1016/j.neuron.2011.04.018 Medline

3. F. Varela, J.-P. Lachaux, E. Rodriguez, J. Martinerie, The brainweb: Phase synchronization and large-scale integration. *Nat. Rev. Neurosci.* **2**, 229–239 (2001). doi:10.1038/35067550 Medline

4. A. E. Motter, S. A. Myers, M. Anghel, T. Nishikawa, Spontaneous synchrony in power-grid networks. *Nat. Phys.* **9**, 191–197 (2013). doi:10.1038/nphys2535

5. L. V. Gambuzza, A. Buscarino, S. Chessari, L. Fortuna, R. Meucci, M. Frasca, Experimental investigation of chimera states with quiescent and synchronous domains in coupled electronic oscillators. *Phys. Rev. E* **90**, 032905 (2014). doi:10.1103/PhysRevE.90.032905 Medline

6. K. Wiesenfeld, P. Colet, S. H. Strogatz, Synchronization transitions in a disordered Josephson series array. *Phys. Rev. Lett.* **76**, 404–407 (1996). doi:10.1103/PhysRevLett.76.404 Medline

7. E. A. Martens, S. Thutupalli, A. Fourrière, O. Hallatschek, Chimera states in mechanical oscillator networks. *Proc. Natl. Acad. Sci. U.S.A.* **110**, 10563–10567 (2013). doi:10.1073/pnas.1302880110 Medline

8. S. Kaka, M. R. Pufall, W. H. Rippard, T. J. Silva, S. E. Russek, J. A. Katine, Mutual phase-locking of microwave spin torque nano-oscillators. *Nature* **437**, 389–392 (2005). doi:10.1038/nature04035 Medline

9. D. P. Rosin, D. Rontani, N. D. Haynes, E. Schöll, D. J. Gauthier, Transient scaling and resurgence of chimera states in networks of Boolean phase oscillators. *Phys. Rev. E* **90**, 030902 (2014). doi:10.1103/PhysRevE.90.030902 Medline

10. R. Roy, K. S. Thornburg Jr., Experimental synchronization of chaotic lasers. *Phys. Rev. Lett.* **72**, 2009–2012 (1994). doi:10.1103/PhysRevLett.72.2009 Medline

11. M. C. Cross, P. C. Hohenberg, Pattern formation outside of equilibrium. *Rev. Mod. Phys.* **65**, 851–1112 (1993). doi:10.1103/RevModPhys.65.851

12. I. Z. Kiss, Y. Zhai, J. L. Hudson, Emerging coherence in a population of chemical oscillators. *Science* **296**, 1676–1678 (2002). doi:10.1126/science.1070757 Medline

13. M. R. Tinsley, S. Nkomo, K. Showalter, Chimera and phase-cluster states in populations of coupled chemical oscillators. *Nat. Phys.* **8**, 662–665 (2012). doi:10.1038/nphys2371

14. X. L. Feng, C. J. White, A. Hajimiri, M. L. Roukes, A self-sustaining ultrahigh-frequency nanoelectromechanical oscillator. *Nat. Nanotechnol.* **3**, 342–346 (2008). doi:10.1038/nnano.2008.125 Medline

15. L. G. Villanueva, R. B. Karabalin, M. H. Matheny, E. Kenig, M. C. Cross, M. L. Roukes, A nanoscale parametric feedback oscillator. *Nano Lett.* **11**, 5054–5059 (2011). doi:10.1021/nl2031162 Medline

16. L. G. Villanueva, E. Kenig, R. B. Karabalin, M. H. Matheny, R. Lifshitz, M. C. Cross, M. L. Roukes, Surpassing fundamental limits of oscillators using nonlinear resonators. *Phys. Rev. Lett.* **110**, 177208 (2013). doi:10.1103/PhysRevLett.110.177208 Medline

17. M. H. Matheny, M. Grau, L. G. Villanueva, R. B. Karabalin, M. C. Cross, M. L. Roukes, Phase synchronization of two anharmonic nanomechanical oscillators. *Phys. Rev. Lett.* **112**, 014101 (2014). doi:10.1103/PhysRevLett.112.014101 Medline

18. Y. Kuramoto, Self-entrainment of a population of coupled non-linear oscillators. In *International Symposium on Mathematical Problems in Theoretical Physics* (Springer, 1975), pp. 420–422.

19. J. A. Acebrón, L. L. Bonilla, C. J. Pérez Vicente, F. Ritort, R. Spigler, The kuramoto model: A simple paradigm for synchronization phenomena. *Rev. Mod. Phys.* **77**, 137–185 (2005). doi:10.1103/RevModPhys.77.137

20. H. Sakaguchi, Y. Kuramoto, A soluble active rotater model showing phase transitions via mutual entertainment. *Prog. Theor. Phys.* **76**, 576–581 (1986). doi:10.1143/PTP.76.576

21. P. Ashwin, J. W. Swift, The dynamics of n weakly coupled identical oscillators. *J. Nonlinear Sci.* **2**, 69–108 (1992). doi:10.1007/BF02429852

22. L. M. Pecora, F. Sorrentino, A. M. Hagerstrom, T. E. Murphy, R. Roy, Cluster synchronization and isolated desynchronization in complex networks with symmetries. *Nat. Commun.* **5**, 4079 (2014). doi:10.1038/ncomms5079 Medline

23. I. Z. Kiss, C. G. Rusin, H. Kori, J. L. Hudson, Engineering complex dynamical structures: Sequential patterns and desynchronization. *Science* **316**, 1886–1889 (2007). doi:10.1126/science.1140858 Medline

24. J. D. Hart, K. Bansal, T. E. Murphy, R. Roy, Experimental observation of chimera and cluster states in a minimal globally coupled network. *Chaos* **26**, 094801 (2016). doi:10.1063/1.4953662 Medline

25. A. A. Temirbayev, Z. Zh. Zhanabaev, S. B. Tarasov, V. I. Ponomarenko, M. Rosenblum, Experiments on oscillator ensembles with global nonlinear coupling. *Phys. Rev. E* **85**, 015204 (2012). doi:10.1103/PhysRevE.85.015204 Medline

26. P. S. Skardal, E. Ott, J. G. Restrepo, Cluster synchrony in systems of coupled phase oscillators with higher-order coupling. *Phys. Rev. E* **84**, 036208 (2011). doi:10.1103/PhysRevE.84.036208 Medline

27. A. Pikovsky, M. Rosenblum, Self-organized partially synchronous dynamics in populations of nonlinearly coupled oscillators. *Physica D* **238**, 27–37 (2009). doi:10.1016/j.physd.2008.08.018

28. P. Clusella, A. Politi, M. Rosenblum, A minimal model of self-consistent partial synchrony. *New J. Phys.* **18**, 093037 (2016). doi:10.1088/1367-2630/18/9/093037

29. P. Ashwin, O. Burylko, Weak chimeras in minimal networks of coupled phase oscillators. *Chaos* **25**, 013106 (2015). doi:10.1063/1.4905197 Medline

30. W. Fon, M. H. Matheny, J. Li, L. Krayzman, M. C. Cross, R. M. D'Souza, J. P. Crutchfield, M. L. Roukes, Complex dynamical networks constructed with fully controllable nonlinear nanomechanical oscillators. *Nano Lett.* **17**, 5977–5983 (2017). doi:10.1021/acs.nanolett.7b02026 Medline

31. M. C. Cross, J. L. Rogers, R. Lifshitz, A. Zumdieck, Synchronization by reactive coupling and nonlinear frequency pulling. *Phys. Rev. E* **73**, 036205 (2006). doi:10.1103/PhysRevE.73.036205 Medline

32. M. C. Cross, A. Zumdieck, R. Lifshitz, J. L. Rogers, Synchronization by nonlinear frequency pulling. *Phys. Rev. Lett.* **93**, 224101 (2004). doi:10.1103/PhysRevLett.93.224101 Medline

33. A. Pikovsky, M. Rosenblum, J. Kurths, *Synchronization: A Universal Concept in Nonlinear Sciences* (Cambridge Univ. Press, 2003).

34. J. Emenheiser, A. Chapman, M. Pósfai, J. P. Crutchfield, M. Mesbahi, R. M. D'Souza, Patterns of patterns of synchronization: Noise induced attractor switching in rings of coupled nonlinear oscillators. *Chaos* **26**, 094816 (2016). doi:10.1063/1.4960191 Medline

35. A. Pikovsky, P. Rosenau, Phase compactons. *Physica D* **218**, 56–69 (2006). doi:10.1016/j.physd.2006.04.015

36. B. Blasius, R. Tönjes, Quasiregular concentric waves in heterogeneous lattices of coupled oscillators. *Phys. Rev. Lett.* **95**, 084101 (2005). doi:10.1103/PhysRevLett.95.084101 Medline

37. M. H. Matheny, L. G. Villanueva, R. B. Karabalin, J. E. Sader, M. L. Roukes, Nonlinear mode-coupling in nanomechanical systems. *Nano Lett.* **13**, 1622–1626 (2013). doi:10.1021/nl400070e Medline

38. D. A. Wiley, S. H. Strogatz, M. Girvan, The size of the sync basin. *Chaos* **16**, 015103 (2006). doi:10.1063/1.2165594 Medline

39. R. L. Honeycutt, Stochastic Runge-Kutta algorithms. I. White noise. *Phys. Rev. A* **45**, 600–603 (1992). doi:10.1103/PhysRevA.45.600 Medline

40. M. C. Soriano, G. Van der Sande, I. Fischer, C. R. Mirasso, Synchronization in simple network motifs with negligible correlation and mutual information measures. *Phys. Rev. Lett.* **108**, 134101 (2012). doi:10.1103/PhysRevLett.108.134101 Medline

41. J. Alexander, G. Auchmuty, Global bifurcations of phase-locked oscillators. *Arch. Ration. Mech. Anal.* **93**, 253–270 (1986). doi:10.1007/BF00281500

42. A. M. Hagerstrom, T. E. Murphy, R. Roy, P. Hövel, I. Omelchenko, E. Schöll, Experimental observation of chimeras in coupled-map lattices. *Nat. Phys.* **8**, 658–661 (2012). doi:10.1038/nphys2372

43. M. J. Panaggio, D. M. Abrams, Chimera states: Coexistence of coherence and incoherence in networks of coupled oscillators. *Nonlinearity* **28**, R67–R87 (2015). doi:10.1088/0951-7715/28/3/R67

44. D. M. Abrams, S. H. Strogatz, Chimera states for coupled oscillators. *Phys. Rev. Lett.* **93**, 174102 (2004). doi:10.1103/PhysRevLett.93.174102 Medline

45. M. J. Panaggio, D. M. Abrams, P. Ashwin, C. R. Laing, Chimera states in networks of phase oscillators: The case of two small populations. *Phys. Rev. E* **93**, 012218 (2016). doi:10.1103/PhysRevE.93.012218 Medline

46. Y. S. Cho, T. Nishikawa, A. E. Motter, Stable chimeras and independently synchronizable clusters. *Phys. Rev. Lett.* **119**, 084101 (2017). doi:10.1103/PhysRevLett.119.084101 Medline

47. R. Grigoriev, M. Cross, H. Schuster, Pinning control of spatiotemporal chaos. *Phys. Rev. Lett.* **79**, 2795–2798 (1997). doi:10.1103/PhysRevLett.79.2795

48. M. Mesbahi, M. Egerstedt, *Graph Theoretic Methods in Multiagent Networks* (Princeton Univ. Press, 2010).

49. T. Coletta, R. Delabays, I. Adagideli, P. Jacquod, Topologically protected loop flows in high voltage ac power grids. *New J. Phys.* **18**, 103042 (2016). doi:10.1088/1367-2630/18/10/103042

50. E. J. Lerner, in *Gravitational, Electric, and Magnetic Forces: An Anthology of Current Thought*, L. C. Krysac, Ed. (Rosen, New York, 2006), pp. 41–50.

51. Y. Susuki, I. Mezić, T. Hikihara, Coherent swing instability of power grids. *J. Nonlinear Sci.* **21**, 403–439 (2011). doi:10.1007/s00332-010-9087-5

52. D. Helbing, Traffic and related self-driven many-particle systems. *Rev. Mod. Phys.* **73**, 1067–1141 (2001). doi:10.1103/RevModPhys.73.1067

53. B. S. Kerner, Autosolitons in applied physics and traffic flow. *AIP Conf. Proc.* **375**, 777–839 (1996). doi:10.1063/1.51016

54. B. S. Kerner, P. Konhäuser, Cluster effect in initially homogeneous traffic flow. *Phys. Rev. E* **48**, R2335–R2338 (1993). doi:10.1103/PhysRevE.48.R2335 Medline

55. I. Omelchenko, A. Provata, J. Hizanidis, E. Schöll, P. Hövel, Robustness of chimera states for coupled FitzHugh-Nagumo oscillators. *Phys. Rev. E* **91**, 022917 (2015). doi:10.1103/PhysRevE.91.022917 Medline

56. B. K. Bera, D. Ghosh, M. Lakshmanan, Chimera states in bursting neurons. *Phys. Rev. E* **93**, 012205 (2016). doi:10.1103/PhysRevE.93.012205 Medline

57. S. Majhi, M. Perc, D. Ghosh, Chimera states in uncoupled neurons induced by a multilayer structure. *Sci. Rep.* **6**, 39033 (2016). doi:10.1038/srep39033 Medline

58. S. Motsch, E. Tadmor, Heterophilious dynamics enhances consensus. *SIAM Rev.* **56**, 577–621 (2014). doi:10.1137/120901866

59. R. Olfati-Saber, J. A. Fax, R. M. Murray, Consensus and cooperation in networked multi-agent systems. *Proc. IEEE* **95**, 215–233 (2007). doi:10.1109/JPROC.2006.887293

60. H. Ronellenfitsch, J. Dunkel, M. Wilczek, Optimal noise-canceling networks. *Phys. Rev. Lett.* **121**, 208301 (2018). doi:10.1103/PhysRevLett.121.208301 Medline

61. R. B. Karabalin, M. H. Matheny, X. L. Feng, E. Defaÿ, G. Le Rhun, C. Marcoux, S. Hentz, P. Andreucci, M. L. Roukes, Piezoelectric nanoelectromechanical resonators based on aluminum nitride thin films. *Appl. Phys. Lett.* **95**, 103111 (2009). doi:10.1063/1.3216586

62. R. B. Karabalin, L. G. Villanueva, M. H. Matheny, J. E. Sader, M. L. Roukes, Stress-induced variations in the stiffness of micro- and nanocantilever beams. *Phys. Rev. Lett.* **108**, 236101 (2012). doi:10.1103/PhysRevLett.108.236101 Medline

63. T. J. Yamaguchi, M. Soma, M. Ishida, T. Watanabe, T. Ohmi, Extraction of instantaneous and rms sinusoidal jitter using an analytic signal method. *IEEE Trans. Circuits Syst. 2* **50**, 288–298 (2003). doi:10.1109/TCSII.2003.812916

64. R. Lifshitz, M. C. Cross, in *Reviews of Nonlinear Dynamics and Complexity*, H. G. Schuster, Ed. (Wiley, 2009), pp. 1–52. doi:10.1002/9783527626359.ch1